UCM1612+1308: a newly identified Blue Compact Galaxy[*]

M. Rego[1], **M. Cordero-Gracia**[1,2], **J. Gallego**[1], **and J. Zamorano**[1]

[1] Departamento Astrofísica, Facultad CC Físicas, Universidad Complutense, E-28040 Madrid, Spain
[2] ETSI Aeronáuticos, Universidad Politécnica, E-28040 Madrid, Spain

Abstract. UCM1612+1308 is a new emission-line galaxy identified in the context of the Universidad Complutense de Madrid (UCM) survey. This object was classified as Blue Compact Galaxy (BCG) from photometric data. A detailed spectroscopic study from new optical observations is presented now. The physical conditions and chemical composition are derived. The ionic abundances yield to a metallicity of $0.23 \pm 0.01\, Z_\odot$ and a very low nitrogen to oxygen abundances ratio, $\log(N/O) = -1.74 \pm 0.07$, supporting a primary nucleosynthesis origin for the nitrogen. The same value has been obtained for the sulfur to oxygen ratio. The comparison of the helium abundance with the oxygen and nitrogen abundances evidences a quickly enrichment of oxygen produced by massive stars. The ionizing cluster has been analyzed yielding a relatively low ionization parameter, $\log \bar{U} = -3$, total number of stars, $\log N^* = 6.18$, stellar mass, $\log M^* = 5.71\, M_\odot$, and gas mass $\log M_g = 7.42\, M_\odot$. A lower limit of the dust mass, $\log M_{dust} = 5.65\, M_\odot$, has been obtained from the IRAS fluxes. The observed data and derived parameters, when interpreted with the evolutionary synthesis models by Leitherer & Heckman (1995), point out to an instantaneous burst with an age of $\log t = 6.7$ yr.

Key words: galaxies: individual (UCM1612+1308) – galaxies: compact – galaxies: abundances – stars: formation

1. Introduction

The UCM Hα survey is an ongoing project to search for star-forming galaxies, with the aim to establish the star formation history of the local universe. The objects are identified by their Hα emission in objective-prism plates. The Schmidt Telescope (Calar Alto Observatory) together with a 4º objective-prism, RG 6330 filter and III aF photographic emulsion, yields a spectral range from $\lambda\lambda$ 6400 to 6850 Å. The program includes follow-up moderate resolution spectroscopy and CCD imaging, and has been described by Zamorano et al. (1994, 1996). Other studies can be found in Rego et al. (1989, 1993, 1994); Gallego et al. (1994, 1995, 1996, 1997); Zamorano et al. (1990a, 1990b, 1992); etc. These results prove that starburst galaxies are the most common type of galaxy identified, some of them showing a moderately low metallicity. UCM1612+1308 is one of the lowest luminosity objects of the sample. In Table 1 we present results from previous photometric studies (Vitores et al. 1996a, 1996b), including apparent, m_r, and absolute, M_r, magnitudes in the Thuan-Gunn band, and the diameter measured at the 24 mag/$\Box$, D_{24}. The absolute magnitude uncertainty has been calculated considering only the apparent magnitude and radial velocity as source of errors. The photometric profile exhibits a bulb component relatively strong. These features, together with the spectral appearance allow us to suspect that UCM1612+1308 is a Blue Compact Galaxy. A more detailed spectral study of this galaxy, considering the object intrinsic properties and in the context of the UCM survey could be useful.

BCGs can supply clues to understand the galaxy evolution scenario. A mostly young stellar population, low metallicity and large gas content support the assumption that these objects are poorly evolved. These features are often used to obtain information on three outstanding points: the origin of the observed nitrogen, the primordial helium abundance and the star-formation modes. Hodge (1989) performed star-forming models in which BCGs undergo just a few brief and strong processes of star formation during their life, while Greggio et al. (1993), among others, have suggested a continuous activity of moderate star formation rate (SFR) with short periods of calmness.

To investigate these problems and to enlarge the baseline of spectroscopic data for BCGs we study in detail UCM1612+1308. The layout of this paper is as follows. The observations and data reduction to obtain emission-line and IRAS fluxes are outlined in Sect. 2. The data are analyzed and the chemical composition including both ionic and helium abundances are obtained in Sect. 3. The ionizing source is investigated in Sect. 4 where the ionization parameter and the mass of the ionized gas and stars are estimated. A study of star-formation

Table 1. UCM1612+1308 basic data

α_{1950}	16 12 57.2
δ_{1950}	+13 08 59
m_r	17.48 ± 0.12
M_r	-16.90 ± 0.15
D_{24} (Kpc)	3
V (km s^{-1})	3630 ± 60

$H_o = 50 \text{km s}^{-1} \text{Mpc}^{-1}$

Table 2. Spectroscopic data of UCM1612+1308

Line	$F(\lambda)/F(H\beta) \times 100$
[O II] $\lambda 3727$	244.3 ± 5.4
[Ne III] $\lambda 3869$	45.0 ± 3.5
He I $\lambda 3889$	19.3 ± 2.7
[Ne III] $\lambda 3968$	21.8 ± 1.7
Hδ $\lambda 4102$	23.4 ± 0.3
Hγ $\lambda 4340$	43.4 ± 0.3
[O III] $\lambda 4363$	6.1 ± 0.3
He I $\lambda 4471$	3.7 ± 0.3
He II $\lambda 4686$	1.4 ± 0.4
Hβ $\lambda 4861$	100.0 ± 0.4
He I $\lambda 4922$	1.0 ± 0.2
[O III] $\lambda 4959$	169.4 ± 0.5
[O III] $\lambda 5007$	523.4 ± 1.4
He I $\lambda 5876$	9.8 ± 0.2
[O I] $\lambda 6300$	3.0 ± 0.2
[S III] $\lambda 6310$	1.6 ± 0.2
[N II] $\lambda 6548$	2.2 ± 0.1
Hα $\lambda 6563$	286.0 ± 0.8
[N II] $\lambda 6584$	7.3 ± 0.2
He I $\lambda 6678$	2.9 ± 0.3
[S II] $\lambda 6717$	15.1 ± 0.3
[S II] $\lambda 6731$	10.7 ± 0.2

$C(H\beta) = 0.008$
$F(H\beta) = (1935.5 \pm 5.0) \times 10^{-17} \text{ erg cm}^{-2} \text{ s}^{-1}$
$EW(H\beta) = 95 \pm 7$ Å
$L(H\beta) = (5.4 \pm 0.1) \times 10^{39} \text{ erg s}^{-1}$

modes and burst age is developed in Sect. 5, using the evolutionary synthesis models from Leitherer & Heckmann (1995). Finally, a rough estimation of the kinetic energy of the burst is performed in Sect. 6 and the discussions are presented in Sect. 7.

2. Observations and data reduction

Spectroscopic observations of UCM1612+1308 were obtained on 1994 July 6 at the 2.5m Isaac Newton Telescope on Roque de los Muchachos Observatory (La Palma, Spain). Long-slit spectra were taken using the IDS Cassegrain spectrograph with the TEK#3 of 1024×1024 pixels CCD. The observations were made using the R900V grating with a 2" slit, providing a spatial scale of 0.71 arsec pixel^{-1} and a dispersion of 1.13 Å/pixel, placed centered in the nucleus with a P.A.= 293°. The seeing was 1"3 FWHM. Two exposures were made covering the spectral ranges $\lambda\lambda\, 3965 - 5325$ Å and $\lambda\lambda\, 5685 - 6955$ Å with 60 minutes integrations. Flat-field and bias corrections were carried out following the standard procedures. The spectra were also corrected from atmospheric extinction using La Palma extinction curves (La Palma Tech. Notes N 69). Flux calibration was made by means of standard stars observed the same night. Observations have been reduced with the FIGARO Package using the standard reduction process. We also have a spectrum of UCM1612+1308 covering the range $\lambda\lambda\, 3700 - 7600$ Å obtained on 1991 June 11. This observation was part of the general follow-up spectroscopy for the UCM survey (Gallego et al. 1996).

The combined spectrum displayed in Fig. 1 shows the typical features of galaxies undergoing global bursts of star formation, with very strong Hα and emission lines arising from high excitation regions, as the complete Balmer series, the [OIII] $\lambda 4363$ and the helium lines. No absorption features are detected and the young stellar population dominates the whole spectrum. The radial velocity, given in Table 1, was calculated as a mean of the all measurable emission-line shifts, weighted with their equivalent widths. The corrected line intensities, extinction coefficient, C(Hβ), together with the Hβ flux, equivalent width and luminosity are given in Table 2.

In addition to the new optical spectra, we also obtained coadded IRAS fluxes at 12, 25, 60 and 100 μm using the NASA/IPAC Extragalactic Database (NED; this data base is operated by the Jet Propulsion Laboratory, California Institute of Technology, under contract with NASA). The flux densities in Janskys in the four bands are: $F_{12} = 0.04$; $F_{25} = 0.12$; $F_{60} = 0.09$:;

$F_{100} = 0.32$:. The FIR flux, in erg cm^{-2} s^{-1}, is defined as (Helou et al. 1988)

$$FIR = 1.26 \times 10^{-11}(2.58F_{60} - F_{100}) \qquad (1)$$

and covers the infrared flux in the range 40–120 μm which represents a fraction of the total infrared emission from a galaxy. The factor 1.26 corrects for the gap between the 60 and 100 band-passes and the filter function. The FIR luminosity is $\log LIR = 8.86 \text{L}_\odot$.

3. Physical conditions and chemical composition

The [OIII]$\lambda 5007$/Hβ ratio is typical of high excitation spectrum and the [OII]$\lambda 3727$/[OIII]$\lambda 5007$ ratio indicates that emission from diffuse interstellar gas can be neglected. Using the Veilleux & Osterbrock (1987) diagrams, the log([OIII]/Hβ) = 0.72 and log([NII]/Hα) = -1.59 values place UCM1612+1308 in the upper left corner where BCGs are preferentially located, in agreement with the above photometric and morphological data.

The identification of the [OI] $\lambda 6300$ line makes evident the emission from predominantly neutral gas, where colliding electrons heated in shock regions can supply the 1.85 eV required to populate the excitation level. A similar mechanism can be used to explain the S$^+$ emission, taking into account its low ionization potential, $\chi_{ion} = 10.4$ eV, in contrast to the N$^+$ emission,
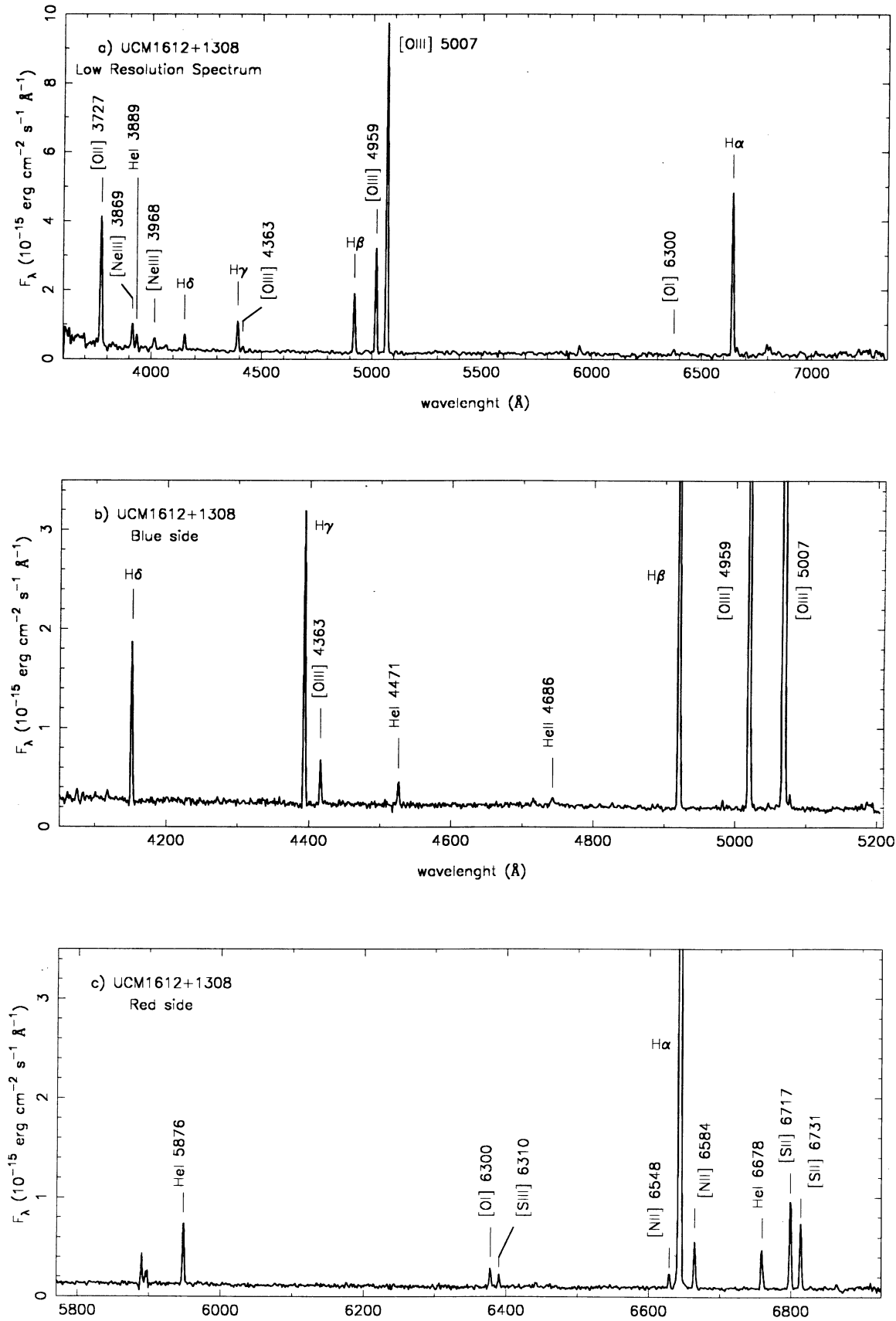
Fig. 1. Spectra of UCM1612+1308

where $\chi_{ion} = 14.6$ eV. Therefore, the [SII] line intensities can be contributed by emissions from neutral and ionized regions. We can estimate the components of both two regions using the relationship obtained by Petuchowski & Bennett (1995) fitting [SII] and [NII] line data measured in 36 SNRs in M33,

$$\frac{I(\text{[SII]})}{I(\text{H}\alpha)} = 0.986 \left(\frac{I(\text{[NII]})}{I(\text{H}\alpha)} \right)^{0.67} + 1.167 \frac{I(\text{[OI]})}{I(\text{H}\alpha)} \qquad (2)$$

The first and second terms on the right-hand side represent the ionized and neutral region contributions respectively. Inserting our observed values into the above equation, it is apparent that the contribution by the neutral region can be neglected, and consequently [SII] and [NII] emissions are correlated.

3.1. Electron temperatures and densities

It has been assumed that ionic emission-lines arises from high-ionization and low-ionization zones with different electron temperatures T_e. The [OIII] and [NIII] lines are originated in the first zone, and the [OII], [NII], [SII] lines are in the second. The $T_e(\text{O}^{++})$ is derived from the [OIII]($\lambda 5007 + \lambda 4959$)/$\lambda 4363$ ratio and the electron number density from [SII] $\lambda 6717/\lambda 6731$ ratio using models from Zamorano & Rego (1985) which provide $T_e(\text{O}^{++}) = 12250 \pm 234$ K and $N_e \simeq 30$ cm^{-3}.

To obtain the low ionization temperature we apply the expression supplied by Dufour et al. (1988) from HII photoionization models

$$T_e(\text{O}^+) = T_e(\text{O}^{++}) - 0.3(T_e(\text{O}^{++}) - 1) \qquad (3)$$

where T_e is in units of 10^4 K, resulting $T_e(\text{O}^+) = 11576 \pm 163$ K.

The [SIII] lines are produced both in low- and high-ionization regions, therefore the temperature, $T_e(\text{S}^{++})$, will be intermediate between $T_e(\text{O}^{++})$ and $T_e(\text{O}^+)$ and it has been derived applying the following expression given by Garnett (1992)

$$T_e(\text{O}^+) = 0.83 \, T_e(\text{O}^{++}) + 0.17 \qquad (4)$$

which provide a value of $T_e(\text{S}^{++}) = 11868 \pm 194$ K.

3.2. Heavy elements abundances

The total abundance for oxygen is computed by means of the expression

$$\frac{\text{O}}{\text{H}} = \frac{\text{O}^+ + \text{O}^{++}}{\text{H}^+} \qquad (5)$$

The identification of the HeII $\lambda 4686$ line points out that part of the oxygen could be in the O^{+++} stage, however its intensity is so weak (11σ above the continuum) that the O^{+++} abundance does not exceed 2% of the total oxygen abundance and can be neglected. Note that levels giving rise to the [OII] lines can be also populated by dielectronic and radiative recombinations. Nevertheless, the efficiency of these processes decrease strongly as the temperature rises, when $T_e > 10000$ K, recombinations contribute less than 1%. Therefore, only collisional excitation has been taken into account.

A significant fraction of the remaining element abundances can be on unseen stages of ionization. In consequence, the total abundance, A, is estimated by inserting an ionization correction factor (ICF) in the following way

$$\frac{A}{\text{H}} = \text{ICF}(A) \frac{A^{+i}}{\text{H}^+} \qquad (6)$$

The only nitrogen lines observed are [NII] $\lambda\lambda 6548$ and 6584. Garnett (1990) has shown that the ICF corresponding to the N/O ratio has a complicated behavior in the case of solar metallicity because of its dependence on the ionization parameter and the effective temperature of the cluster. However, for lower abundances, the approach N/O = N$^+$/O$^+$ seems to have an accuracy better than 20%. No more information can be drawn for neon. Since it is observed as Ne^{++} we use an ICF(Ne) = O/O^{++}.

Sulfur is found in two ionization stages, S$^+$ and S^{++}. The photoionization models evidence that S^{++} is the dominant ion, concentrating about 60% of the total sulfur abundance of the nebula. Unfortunately we observe only [SIII] $\lambda 6310$ which, as usual in HII regions, is weak and very sensitive to the temperature. Garnett (1989) assumes that in low abundance objects and highly excited conditions, the ICF(S) is depending on the ionization fraction O$^+$/O and can be expressed by

$$\begin{aligned} \text{ICF(S)} = \text{S}/(\text{S}^+ + \text{S}^{++}) = \{0.013 + x(5.10 + \\ x(-12.78 + x(14.77 - 6.11x)))\}^{-1} \end{aligned} \qquad (7)$$

where $x = \text{O}^+/\text{O}$. Then we have

$$\frac{\text{S}}{\text{H}} = \text{ICF(S)} \frac{N(\text{S}^+ + \text{S}^{++})}{N(\text{H}^+)} \qquad (8)$$

The ionic abundances were calculated using the nebular package (Shaw & Dufour 1995). Total abundances are listed in Table 3.

The metallicity of UCM1612+1308 relative to the solar value is $Z_{obs}/Z_{\odot} = (\text{O/H})_{obs}/(\text{O/H})_{\odot} = 0.23 \pm 0.01$. Taking into account this value, the oxygen to nitrogen abundances ratio, $\log(\text{N/O}) = -1.74 \pm 0.07$, is rather low compared to the values provided by the literature. To see this, we plotted $\log(\text{N/O})$ vs $12 + \log(\text{O/H})$ using recent data from HII galaxies with $12 + \log(\text{O/H}) < 8.3$. A large scatter and a mean of $\log(\text{N/O}) = -1.44 \pm 0.26$ results, confirming those obtained by other authors (e.g. Kunth & Sargent 1983; Garnett 1990). Nevertheless when HII galaxies with higher metallicity, $12 + \log(\text{O/H}) > 8.3$, are plotted, the data points can be fitted by a linear relationship, but the BCGs continue displaying an important scatter (Storchi-Bergmann et al. 1994).

A study of the S/O and O/H relationship using statistically significant samples is limited because of the lack of S^{++} abundances in many objects. Results from Garnett (1989) using a small sample seem to indicate that S/O does not vary systematically with metallicity. Some information however may be obtained from the models of Arnett (1978), as plotted by Garnett (1989) in a $\log(\text{S/O})$ vs $12 + \log(\text{O/H})$ diagram. Inserting $\log(\text{S/O}) = -1.74$, UCM1612+1308 is located between the lines corresponding to the slopes 2 and 3 of the initial mass function.

Table 3. Abundances of UCM1612+1308

	Abundances
$10^5\,O^+/H^+$	5.05 ± 0.11
$10^5\,O^{++}/H^+$	9.87 ± 0.49
$10^4\,O/H$	1.49 ± 0.05
$12 + \log(O/H)$	8.17 ± 0.03
$10^7\,N^+/H^+$	9.21 ± 0.47
$10^6\,N/H$	2.72 ± 0.18
$12 + \log(N/H)$	6.43 ± 0.06
$10^5\,Ne^{++}/H^+$	2.23 ± 0.25
$10^5\,Ne/H$	3.37 ± 0.43
$12 + \log(Ne/H)$	7.53 ± 0.13
$10^7\,S^+/H^+$	3.81 ± 0.10
$10^7\,S^{++}/H^+$	18.92 ± 2.36
$10^6\,S/H$	2.96 ± 0.37
$12 + \log(S/H)$	6.47 ± 0.12
$(O/H)_\odot = 6.6069 \times 10^{-4}$	

3.3. Helium abundance determination

The total abundance of helium is determined by

$$\frac{He}{H} = \frac{He^o + He^+ + He^{++}}{H^+} \qquad (9)$$

Since UCM1612+1308 exhibits a high degree of ionization, the neutral helium fraction can be neglected. We have identified the HeI $\lambda4471$, $\lambda5876$, $\lambda6678$ lines and HeII $\lambda4686$ line. The $\lambda6678$ line is more reliable than the commonly measured $\lambda4471$ and $\lambda5876$ lines. First, because it is less subject to effects of underlying absorption and collision and radiative effects and, second, because it is virtually free of reddening and calibration uncertainties. The HeII $\lambda4686$ line has been observed in several low abundance high excitation nebulae, however it has never been certain whether this line has nebular or circumstellar origin. Following Skillman & Kennicutt (1993) we will assume that all the He emission is nebular.

Considering the observed electron temperature, there are mainly two physical mechanisms that can make the He line intensities deviate from pure recombination values: self-absorption, prevalent in the HeI $\lambda3889$ line, and collisional excitation from the metastable 2^3S and 2^1S levels of HeI which can also produce the enhancement of some helium lines. Self-absorption should cause a decrease of the $\lambda3889$ intensity. However, if we subtract from this feature the H8 line, which theoretical recombination intensity is about 0.1 of the Hβ intensity, the ratio between the corrected feature and the $\lambda4471$ line intensities is 2.5. This result is close to 2.4, the theoretical value. We conclude that the effect of self-absorption on HeI intensities can be neglected.

We turn next to discuss the correction of the HeI collisional excitation, γ, which is defined as,

$$y^+ = \frac{y^+(\text{uncorrected})}{1 + \gamma} \qquad (10)$$

The enhancement factor, $1 + \gamma$, has been evaluated from the formulae provided by Clegg (1987). The intensities in the case of pure recombination are given by

$$I_r = I_{obs}/(1 + \gamma) \qquad (11)$$

Since $(1+\gamma)$ values range from 1.002 to 1.004, the collisional correction can be neglected in all cases and we can assume a pure recombination.

To determine the helium abundance we applied the analytical approximations provided by Kunth & Sargent (1983), based in the theoretical recombination emissivities of Brocklehurst (1971, 1972). We obtain

$$
\begin{aligned}
y^+(4471) &= (7.75 \pm 0.63) \times 10^{-2} \\
y^+(5876) &= (7.59 \pm 0.15) \times 10^{-2} \\
y^+(6678) &= (7.88 \pm 0.81) \times 10^{-2} \\
y^+(\text{mean}) &= (7.74 \pm 0.35) \times 10^{-2} \\
y^{++} &= (1.21 \pm 0.35) \times 10^{-3}
\end{aligned}
\qquad (12)
$$

The correction factor for neutral helium was estimated applying the following relation obtained from photoionization models (Stasinska 1990),

$$ICF(He^o) = 1.00 + \eta(0.005 + 0.001\eta) = 1.0028 \qquad (13)$$

where η is the radiation softness parameter as defined by Vilchez & Pagel (1988). This value confirms that the correction factor does not exceed 1%, as occurs for all BCGs (Izotov et al. 1994). Finally the helium mass fraction is

$$Y = \frac{4y\left[1 - 20(O/H)\right]}{1 + 4y} = 0.24 \pm 0.01 \qquad (14)$$

lower than the expected value from the observed metallicity but consistent with the nitrogen abundance. We will discuss this result later.

4. The ionizing source

4.1. The ionization parameter and effective temperature

The total number of H-ionizing photons ($\lambda < 912$ Å), $Q(H^o)$, emitted per second by a stellar population within a region is related to the observed luminosity (after correction of extinction) by

$$Q(H^o) = \frac{\alpha_B\,\lambda_H}{\alpha_H^{\text{eff}}\,hc}\,L(H\beta) = 1.42 \times 10^{52} \quad \text{photons s}^{-1} \qquad (15)$$

where α_B is the hydrogen case B recombination coefficient to all levels above the ground level. α_H^{eff} and $L(H\beta)$ are the effective recombination coefficient and the luminosity of the Hβ line, respectively. This equation assumes that the region of interest

is an ideal HII region: dust-free and completely optically thick to Lyman continuum radiation (case B ionization).

In a similar way, the total number of He-ionizing photons $(505 > \lambda > 228\,\text{Å})$ has been computed from the HeI $\lambda4471$, $\lambda5876$ and $\lambda6678$ lines using the following expression

$$Q(\text{He}^{\text{o}}) = \frac{\alpha_{\text{B}}}{\alpha_{\text{He}}^{\text{eff}}} \frac{\lambda_{\text{He}}}{hc} \text{L(He)} \tag{16}$$

The mean value corresponding to the three lines is $Q(\text{He}^{\text{o}}) = 1.48 \times 10^{51}$ photons s^{-1}.

The ionization parameter, U, is the ratio of photons to electrons in the gas and is related to the level of the ionization of the gas. Several authors have remarked that U and O/H are anticorrelated (e.g. Evans & Dopita 1985; Campbell 1988). A mean ionization parameter (dimensionless), $\bar{\text{U}}$, is defined as

$$\bar{\text{U}} = \frac{3\, Q(\text{H}^{\text{o}})}{4\pi\, N_e \text{R}_\text{s}^2 c} \tag{17}$$

where the Strömgren radius, R_s, is given by

$$\text{R}_\text{s} = \left(\frac{3\, Q(\text{H}^{\text{o}})}{4\pi\, f\, N_e^2 \alpha_{\text{B}}}\right)^{1/3} \tag{18}$$

and the filling factor, f, is obtained from

$$\text{V}_\text{s} f = \frac{4\pi}{3}\text{R}_\text{s}^3 f = \frac{\text{L(H}\beta)}{\text{j(H}\beta)} \tag{19}$$

which provide a value of $f = 1.8 \times 10^{-3}$. By substituting, the ionization parameter is expressed in the form

$$\bar{\text{U}} = \frac{1}{c}\left(\frac{3}{4\pi} Q(\text{H}^{\text{o}})\alpha_{\text{B}}^2 N_e\, f^2\right)^{1/3} \tag{20}$$

resulting a value of $\log \bar{\text{U}} = -3.00$

The determination of the ionization parameter presents uncertainties hard to evaluate. It is strongly dependent on the filling factor, age and metallicity of the ionizing cluster as well as on the mass, density and distribution of the ionized gas. These properties are not the same in BCGs than in other other types of HII galaxies. Consequently, the interpretation of $\bar{\text{U}}$ in the context of the present ionization models can be ambiguous. Campbell (1988) has plotted, in a $\log \bar{\text{U}}$ vs $\log(\text{O/H})$ diagram, $\bar{\text{U}}$ data from a sample of HII galaxies with $\log(\text{O/H})$ covering -3.6 to -4.4. The data points are largely scattered but it is apparent a trend showing an anti-correlation between $\bar{\text{U}}$ and metallicity. When UCM1612+1308 is placed in this diagram it appears in a position rather lower than objects with similar O/H abundance. Note that BCGs with similar O/H abundances than UCM1612+1308 show a large dispersion when placed in this diagram.

The effective temperature of the cluster, T_{cl}, ruling the photoionization, is defined by Lequeux et al. (1981) as the temperature of a star producing the same $Q(\text{He}^{\text{o}})/Q(\text{H}^{\text{o}})$ ratio than the observed one. Using data derived by Mayya (1995) results a $T_{\text{cl}} \approx 37500\,\text{K}$.

4.2. The starburst population

The total number of ionizing photons, Q, needed to explain the observed luminosity is related with the number of ionizing photons coming from stars of mass m, $Q^*(m)$, by the equation

$$Q = \int_{0.1}^{100} Q^*(m)\phi(m)\, dm \tag{21}$$

where $\phi(m)$ is the initial mass function (IMF) and the IMF slope, α, is assumed to be the standard value $\alpha = 2.35$. Since the $Q(\text{He}^{\text{o}})/Q(\text{H}^{\text{o}})$ ratio in the main sequence stars decrease exponentially with the mass, we consider that only photons with $\lambda \leq 505\,\text{Å}$ are effective to photoionize the gas. The total number of stars, N^*, and stellar mass, M^*, required to interpret the total number of ionizing photons are given by the following expressions

$$N^* = Q(\text{H}^{\text{o}})\frac{\int_{0.1}^{100} \phi(m)\, dm}{\int_{0.1}^{100} Q^*(m)\phi(m)\, dm} \tag{22}$$

$$M^* = Q(\text{H}^{\text{o}})\frac{\int_{0.1}^{100} m\, \phi(m)\, dm}{\int_{0.1}^{100} Q^*(m)\phi(m)\, dm}$$

$Q^*(m)$, in number s^{-1}, was drawn from the models of Kurucz (1992) with solar metallicity because $Q^*(m)$ starts to depend significantly on metallicity when $Z = 0.05Z_\odot$ and the stellar mass is lower than $8\,\text{M}_\odot$. However these stars do not contribute appreciably to the total number of ionizing photons. From the above equations it results, $N^* = 1.5 \times 10^6$ and $M^* = 5.1 \times 10^5\,\text{M}_\odot$.

The fraction of equivalent stars O7V, N_{OV}, that is, with an effective temperature being the same as the cluster, is given by

$$\frac{N_{\text{OV}}}{N^*} = \frac{\int_{0.1}^{100} Q^*(m)\,\phi(m)\, dm}{Q_{\text{OV}} \int_{0.1}^{100} \phi(m)\, dm} = 3.8 \times 10^{-3} \tag{23}$$

4.3. Mass of the ionized gas

The mass of the emitting gas can be estimated by

$$M_{gas} = (N_p\, m_p + N_{\text{He}} m_{\text{He}})\text{V}\, f \simeq 1.4\, N_p\, m_p \frac{\text{L(H}\alpha)}{\text{j(H}\alpha)} \tag{24}$$

Assuming the case B (Osterbrock 1989). For $N_{\text{He}} = 0.1 N_p$ and $N_e = N_p + 1.5 N_{\text{He}}$, we have $M_{gas} = 2.6 \times 10^7\,\text{M}_\odot$, which must be considered only a lower limit.

4.4. Mass of dust

The dust mass, M_{dust}, is estimated from the following expression given by Young et al. (1989)

$$M_{dust} = 4.78 F_{100}\text{D}^2\{\exp(143.88/T_{dust}) - 1\} \tag{25}$$

M_{dust} is in $\text{M}_\odot$, F_{100} is in Jy, D is in Mpc and the dust temperature is in K. We adopt a graphite grain opacity of

$K_{100\mu m} = 25\,\mathrm{cm^2\,g^{-1}}$ (Hildebrand 1983) yielding to the factor 4.78. T_{dust} was derived by introducing the F_{100}/F_{60} observed ratio in Table B.1 of Cataloged Galaxies and Quasars Observed in the IRAS Survey, assuming a single temperature component and a λ^{-1} emissivity law. In this way a $T_{dust} = 31.3\,\mathrm{K}$ is obtained. By substituting in the above expression results a $\log M_{dust} = 5.65\,\mathrm{M_\odot}$. Since the warm luminosity measured by IRAS is powered primarily by O and B stars, only some of the dust at 30 K may be heated and a large fraction will be colder than 30 K, radiating predominantly at wavelengths beyond $120\,\mu$m.

5. The kinetic energy of the burst

In order to evaluate the mechanical energy liberated by massive stars we take into account contributions from supernova explosions, mass loss of massive stars in the main-sequence and Wolf-Rayet stages. The last was included considering the detection of the HeII $\lambda 4686$ line in the observed spectrum. The total kinetic energy is

$$
\begin{aligned}
E_k = E_{\mathrm{SN}} + E_{\mathrm{WR}} + E_{\mathrm{MS}} = \\
< E_{\mathrm{SN}} > \int_{m_i}^{100} \phi(m)\,dm + \\
\tfrac{1}{2} \int_{m_i}^{100} \phi(m)\,\dot m_w\, t_{\mathrm{MS}}\, V_w^2\,dm + < E_{\mathrm{WR}} > \int_{25}^{100} \phi(m)\,dm
\end{aligned}
\tag{26}
$$

where $< E_{\mathrm{SN}} >= 7.5 \times 10^{50}$ erg is the mean energy liberated in both Type I and II supernovae (Chevalier 1977); $< E_{\mathrm{WR}} >= 5 \times 10^{50}$ erg (Abbott 1982) is the wind mean energy of the W-R stars. We took a low mass limit of $33\,\mathrm{M_\odot}$ to determine the number of SN, in consistence with the burst age.

The mass-loss rate, $\dot m_w$, main-sequence lifetime, t_{MS}, and wind velocity, V_w, are estimated by (Elson et al. 1989)

$$
\begin{aligned}
\dot m_w &= 5.76 \times 10^{-15}\, m^5 \quad (\mathrm{M_\odot\,yr^{-1}}) \\
t_{\mathrm{MS}} &= 1.20 \times 10^8\, m^{-0.9} \quad (\mathrm{yr}) \\
V_w &= 1.86 \times 10^8\, m^{0.14} \quad (\mathrm{cm\,s^{-1}})
\end{aligned}
\tag{27}
$$

The kinetic energy produced in the burst is therefore approximately $E_k = 1.5 \times 10^{54}$ erg.

6. Modeling the starburst

Information about the burst age and star-formation modes is achieved using the Leitherer & Heckmann (1995) sets of evolutionary synthesis models. They offer among other advantages, a suitable metallicity and IMF slope ranges. Particularly those with Z=0.25 $Z_\odot$ and $\alpha = 2.35$ have been retained, and also two formation modes. One, is the instantaneous burst whose duration is short compared to the age and where all stars are formed suddenly and not subsequent star formation is produced. The other, is the constant star formation with time.

The input parameters are the ionizing photons, $Q(\mathrm{H^o})$ and $Q(\mathrm{He^o})$, and the equivalent widths of Hβ and Hα. The constant star-formation model provides ages ranging from $\log t = 1.7$ to 7.1 years so this mode has been discarded. However, the instantaneous burst model leads to closer values: $\log t = 6.6$ (EW(Hβ), EW(Hα), E_k), 6.7 ($Q(\mathrm{H^o})$) and 6.8 ($Q(\mathrm{He^o})$) years.

This mode explains the observed properties and therefore, at the present time, the burst has finished and the star population is coeval.

The Hα luminosity also provides information about the SFR when the star formation is ongoing at a constant rate. We can obtain an indicative information about this equivalent SFR from the expression (Kennicutt 1983)

$$
\mathrm{SFR} = 5.45 \times 10^{-9}\, \mathrm{L(H\alpha)} \ (\mathrm{L_\odot}) = 0.02\,\mathrm{M_\odot\,yr^{-1}}
\tag{28}
$$

where a lower mass limit of $10\,\mathrm{M_\odot}$ is assumed. Inserting the age of the burst instead the burst duration, as an upper limit, a stellar mass of $1.14 \times 10^5\,\mathrm{M_\odot}$ results, which is very close to that computed in Sect. 4.2.

7. Summary and conclusions

We have performed a study of the properties of the UCM1612+1308 galaxy. We find a high excitation spectrum, moderately low metallicity and relatively high gas content which are in agreement with its photometric classification as a BCG.

From the nebular emission lines, gas abundances are calculated. A low oxygen abundance, $12 + \log(\mathrm{O/H}) \approx 8.2$, is obtained. The N/O abundance ratio, $\log(\mathrm{N/O}) = -1.74$, is one of the lowest known. This value may indicate an enrichment of the interstellar gas by nitrogen mainly produced by primary nucleosynthesis in high and intermediate mass stars. This result, together with the low oxygen abundance, discards a continuous star formation and leads to the assumption of a high efficiency in oxygen rich stars generation by the present and previous bursts.

The sulfur to oxygen abundances ratio obtained is also low, and equal to the N/O ratio. As nitrogen, sulfur is a product of primary nucleosynthesis but the S/O ratio increases inversely to the supernovae energy, which rises with the stellar mass. Therefore, this ratio can be related with the evolution of stars having a high and intermediate mass. To interpret our S/O ratio we can not refer to data compiled from literature, which offers little information due to the large dispersion and uncertainties, mainly caused by the S^{++} abundances. Some evidence comes from Garnett (1990) who plots $\log(\mathrm{S/O})$ against $12+\log(\mathrm{O/H})$ using nucleosynthesis models of Arnett (1978). The UCM1612+1308 appears placed between the lines corresponding to the initial mass function slopes $\alpha = 2$ and 3.

It is instructive to compare the O/H and N/H abundances against the helium abundance. Inserting our data into the Y vs O/H and Y vs N/H diagrams built by Izotov et al. (1994), whom plot low metallicity BCGs data, UCM1612+1308 appears, in the first diagram into the external region bounded by the -1σ limit of the regression line. Whereas in the second one, is on the regression line.

These results seem to point out differences between the oxygen and nitrogen enrichment rates. It is known that oxygen is produced by massive stars ($M > 8\,\mathrm{M_\odot}$), while primary nitrogen is synthesized by intermediate mass stars ($3\,\mathrm{M_\odot} < M < 8\,\mathrm{M_\odot}$) experiencing an envelope burning, and helium, by stars with any initial mass. Therefore, if massive stars are prevailing in the UCM1612+1308 burst, the gas is quickly enriched

with oxygen. Nevertheless the nitrogen and helium abundances change much more slowly.

The lack of [SII] emission from the neutral gas established in Sect. 2 can be explained by the low sulfur abundance. Being sulfur and nitrogen emission intensities correlated, enrichment by these elements is less efficient than oxygen in both ionized and neutral regions. These results, together with the helium abundance obtained, suggest that sulfur and nitrogen abundances are more significant indicators of the burst age than oxygen.

The above results support the election of the Leitherer & Heckmann (1995) models with a metallicity of $0.25\,Z_\odot$, an upper mass limit of $100\,M_\odot$ and slope of the initial mass function of $\alpha = 2.35$. Inserting the observational data and derived parameters, it is clear that constant-star formation must be excluded and UCM1612+1308 has undergone an instantaneous starburst of age $\log t = 6.7$ yr.

References

Abbott D.C. 1982, ApJ 263, 723
Arnett W.D. 1978, ApJ 219, 1008
Brocklehurst M. 1971, MNRAS 153, 471
Brocklehurst M. 1972, MNRAS 157, 211
Campbell A. 1988, ApJ 335, 644
Chevalier R. 1977, ARA&A 15, 175
Clegg R.E.S. 1987, MNRAS 229, 31p
Dufour R.J., Garnett D.R., Shields G.A. 1988, ApJ 332, 752
Elson R.A.W., Fall S.M., Freeman K.C. 1989, ApJ 336, 734
Evans I.N. & Dopita M.A. 1985, ApJS 58, 125
Gallego J., Zamorano J., Rego M., Vitores A.G. 1994, A&A 290, 705
Gallego J., Zamorano J., Aragón-Salamanca A., Rego M. 1995, ApJ 455, L1
Gallego J., Zamorano J., Rego M., Alonso O., Vitores A.G. 1996, A&AS 120, 323
Gallego J., Zamorano J., Rego M., Vitores A.G. 1997, ApJ 475, 502
Garnett D.R. 1989, ApJ 345, 282
Garnett D.R. 1990, ApJ 363, 142
Garnett D.R. 1992, AJ 103, 1330
Greggio L., Marconi G., Tosi M., Focardi P. 1993, AJ 105, 894
Helou G., Khan I., Malek L., Boehmer L. 1988, ApJS 68, 151
Hildebrand R.H. 1983, QJRAS 24, 267
Hodge P. 1989, ARA&A 27, 139
Izotov Y.I., Thuan T.X., Lipotvetsky V.A. 1994, ApJ 435, 667
Kennicutt R.C. 1983, ApJ 272, 54
Kunth D. & Sargent W.L.W. 1983, ApJ 273, 81
Kurucz R.L. 1992, in IAU Symp. 149, The Stellar Populations of Galaxies, ed. B. Barbuy & A. Renzini (Dordrecht: Kluwer), p225
Leitherer C. & Heckmann T.M. 1995, ApJS 96, 9
Lequeux J., Maucherat-Joubert M., Deharveng J.M., Kunth D. 1981, A&A 103, 305
Mayya Y.D. 1995, AJ 109, 2503
Osterbrock D.E. 1989 in Astrophysics of Gaseous Nebulae and Active Galactic Nuclei, Mill Valley, C.A. University Science Books
Petuchowski S.J. & Bennett C.L. 1995, ApJ 438, 735
Rego M., Zamorano J., Gonzalez-Riestra R. 1989, A&AS 79, 443
Rego M., Cordero-Gracia M., Zamorano J., Gallego J. 1993, AJ 105, 427
Rego M., Zamorano J., Gallego J., Vitores A.G. 1994, A&A 281, 348
Shaw R.A. & Dufour R.J. 1995, PASP 107, 896
Skillman E.D. & Kennicutt R.C. 1993, ApJ 411, 655
Stasinska G. 1990, A&AS 83, 501
Storchi-Bergmann T., Calzetti D., Kinney A.L. 1994, ApJ 429, 572
Veilleux S. & Osterbrock D.E. 1987, ApJ 63, 295
Vilchez J.M. & Pagel B.E.J. 1988, MNRAS 231, 257
Vitores A.G., Zamorano J., Rego M., Alonso O., Gallego J. 1996a, A&AS 118, 7
Vitores A.G., Zamorano J., Rego M., Gallego J., Alonso O. 1996b, A&AS 120, 38
Young J.S., Xie S., Kenney J.D.P., Rice W.L. 1989, ApJS 70, 699
Zamorano J. & Rego M. 1985, A&AS 62, 173
Zamorano J., Rego M., Rodriguez G., Gonzalez-Riestra R. 1990a, Ap&SS 170, 353
Zamorano J., Rego M., GonzalezRiestra R., Rodriguez G. 1990b, Ap&SS 170, 533
Zamorano J., Gallego J., Rego M., Vitores A.G., Gonzalez-Riestra R. 1992, AJ 104, 1000
Zamorano J., Rego M., Gallego J., Vitores A.G., Gonzalez-Riestra R., Rodriguez G. 1994, ApJS 95, 387
Zamorano J., Gallego J., Rego M., Vitores A.G., Alonso O. 1996, ApJS 105, 343